JOURNAL OF APPLIED ELECTROCHEMISTRY 24 (1994) 310–315

Kinetics and mechanism of the oxygen evolution reaction at oxide-coated Co–Ni amorphous alloy electrodes

T. KESSLER

Facultad de Ingeniería, Universidad Nacional del Centro de la Provincia de Buenos Aires, Casilla de Correo 12, 7400 Olavarría, Argentina

W. E. TRIACA, A. J. ARVIA

Instituto de Investigaciones Fisicoquímicas Teóricas y Aplicadas (INIFTA), Facultad de Ciencias Exactas, Universidad Nacional de La Plata, Sucursal 4, Casilla de Correo 16 (1900) La Plata, Argentina

Received 16 March 1993; revised July 1993

Oxygen evolution reaction (o.e.r.) kinetics in NaOH solutions have been studied on both fresh and oxide covered $Co_{50}Ni_{25}Si_{15}B_{10}$ amorphous alloy (G-16) electrodes. Steady state polarization curves obtained in different aqueous xM NaOH ($0.1 \leqslant x \leqslant 4$) in the 30–80° C range fulfill Tafel relationships at low overpotentials; the Tafel slope is close to $2.3(RT/F)$ V dec^{-1} for both G-16 and oxide coated G-16 electrodes. At high overpotentials, ohmic relationships with slopes becoming increasingly steep, regardless of the NaOH concentration, are observed. In the Tafel region, the reaction order with respect to OH^- is near 2. The apparent current density at constant potential, for oxide coated G-16 electrodes, is greater than that for uncoated G-16. The high catalytic activity of the oxide coated G-16 for the o.e.r. is attributed to its spinel-type structure. The kinetics of the o.e.r. at low overpotentials is explained through a mechanism involving a first electron transfer step followed by a rate-determining chemical step.

1. Introduction

In an attempt to increase the anode efficiency in alkaline water electrolysis, new materials are being sought. In particular, amorphous alloys show unusual corrosion resistance in alkaline solutions, as well as a high surface area and good catalytic activity for the o.e.r. [1–9].

The $Co_{50}Ni_{25}Si_{15}B_{10}$ amorphous alloy commercially known as G-16, has been identified as an efficient electrocatalyst for the o.e.r. in alkaline solution as its catalytic activity is comparable to that of platinum or nickel [5, 6]. Kinetic data for the o.e.r. on amorphous and crystalline Ni–Co alloys in aqueous alkaline solution has been reported [5, 6, 8, 9]. The electrocatalytic properties of G-16 can be improved when it is coated with a hydrous mixed oxide layer produced by applying a repetitive square wave potential (r.s.w.p.) routine in alkaline solution [10]. The oxide coated G-16 electrodes resulting from this method are very reproducible in behaviour. The composition of the oxide coating corresponds to a $NiCo_2O_4$-spinel [10].

The o.e.r. at G-16 has been studied by electrochemical impedance spectroscopy (EIS) [11] and a possible mechanism for the reaction has been proposed.

The aim of this work is to investigate the behaviour of hydrous oxide film covered G-16 electrodes for the o.e.r. in alkaline solutions. The kinetic data reported in this work, together with structural information of the oxide coating, allow the suggestion of a mechanism for the o.e.r. at low overpotentials and an explanation of the ohmic-type characteristics of the OER at high overpotentials.

2. Experimental details

The working electrodes consisted of ribbons of $Co_{50}Ni_{25}Si_{15}B_{10}$ amorphous alloy (G-16, Vakuummschmelze Hanau, GmbH) about 1 cm^2 in geometric area. Oxide layers were grown on the specimens by applying a r.s.w.p. routine between an upper potential limit, $E_u = 1.0$ V, and a lower potential limit, $E_l = -1.0$ V, at frequency $f = 0.6$ kHz for time $t = 1$ min [10]. The experimental setup, the sample preparation and the characterization of the oxide films have been described elsewhere [10]. Experiments were performed in aqueous xM NaOH ($0.1 \leqslant x \leqslant 4$) in the $30° C \leqslant T \leqslant 80° C$ range. A conventional three electrode cell was used employing a platinum counter electrode and a hydrogen electrode in the same solution as the reference electrode. Potentials in the text are referred to the reversible hydrogen electrode (RHE) in the same electrolyte solution, unless otherwise stated.

The relative increase in active surface area of the working electrode due to the application of the r.s.w.p. routine was estimated through the operational roughness factor R, defined as $R = Q_a/Q_b$, where Q_a and Q_b are the overall voltammetric

0021-891X 1994 Chapman & Hall

charges obtained from voltammograms run in xM NaOH at $0.1\,V\,s^{-1}$ between 0.05 and 1.55 V, after and before applying the r.s.w.p. routine, respectively [10].

Prior to the polarization experiments, the oxide film coated G-16 electrodes were stabilized by a 10 min potential cycling at $0.1\,V\,s^{-1}$ between 0.05 and 1.55 V. Steady and potentiodynamic potential (E) against apparent current density (j) curves were made. The latter were run in the $1.4V \leqslant E \leqslant 1.9\,V$ range at $10^{-4}\,V\,s^{-1}$. The apparent current density is given with respect to the geometric area of the working electrode. The ohmic resistance of the solution between the end of the capillary tip of the reference electrode and the working electrode was 6.3 and 0.5 Ω for 0.1 and 1 M NaOH, respectively.

To compare the true electrocatalytic activity of G-16 and oxide coated G-16 electrodes for the o.e.r., the values of j must be referred to the real electrode surface area. This was achieved through the apparent capacitive current densities [12]. Accordingly, cyclic voltammograms were recorded from 0.25 to 0.30 V, i.e., within the small potential window where faradic processes are, apparently, absent to allow us to obtain the double layer capacitance, according to the method described elsewhere [12].

SEM micrographs of working electrode surfaces were obtained before and after the o.e.r. polarization experiments.

3. Results

The j against v plots from G-16 and oxide coated G-16 anodes ($R = 30$) of same apparent geometric area in the 0.25 to 0.30 V range approach a linear relationship for $v < 0.08\,V\,s^{-1}$ (Fig. 1). The slope of the linear portion increases from G-16 to oxide coated G-16. From the comparison of these slopes [13], it appears that the oxide coated G-16 active surface area is 1.4 times greater than that of G-16. The corrected current density is denoted as j^* in the plots and tables.

Typical polarization curves for o.e.r. in 1 M NaOH

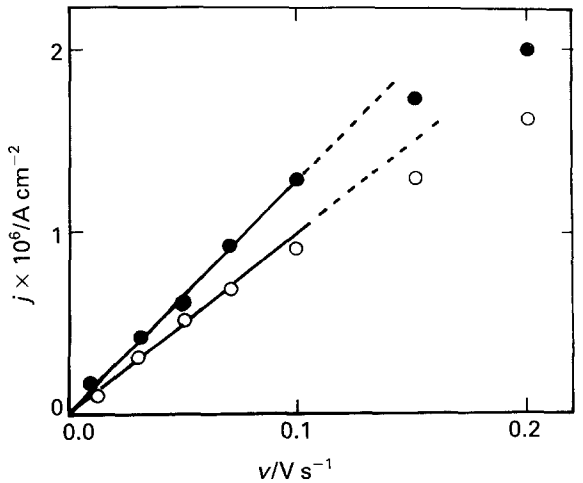

Fig. 1. Current density dependence on potential sweep rate at 0.25 V. 1 M NaOH, 30° C. Untreated G-16 (○); oxide coated G-16 (●).

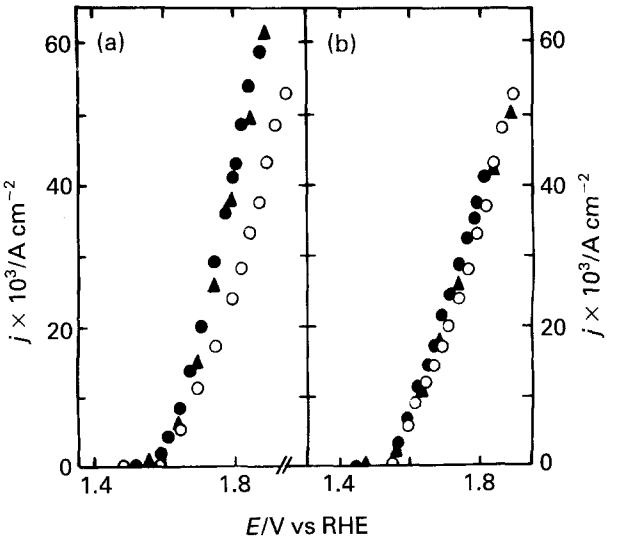

Fig. 2. O.e.r. polarization curves. 1 M NaOH, 30° C. Untreated G-16 (○); oxide coated G-16, $R = 20$ (▲), $R = 30$ (●). (a) E against j (apparent current density) plot; (b) E against j^* (corrected current density) plot.

at 30° C at G-16 and oxide coated G-16 of thicknesses ranging from 30 to 50 nm [10] ($20 \leqslant R \leqslant 30$) are shown in Fig. 2(a). At constant potential the values of j, expressed either as j (Fig. 2(a)) or j^* (Fig. 2(b)) for oxide coated G-16, are much greater than those corresponding to G-16. These results also suggest there is no specific effect of R on the catalytic activity of oxide coated G-16 for the o.e.r.

3.1. *Tafel region*

Polarization curves with oxide coated G-16 electrodes ($R = 30$) at different NaOH concentrations and temperatures result in linear E against $\log j^*$ relationships (Tafel regions) in the 1.4–1.6 V range regardless of the experimental conditions (Fig. 3). The linear portion range decreases as both NaOH concentration and temperature are decreased.

In 1 M NaOH, at 30° C, Tafel slopes of $0.06\,V\,dec^{-1}$ were obtained for both G-16 and oxide coated G-16. The Tafel slopes (b_T) and the apparent exchange current densities (j_0^*) from the extrapolation of the linear plot to the corresponding reversible oxygen electrode potential for oxide coated G-16 under

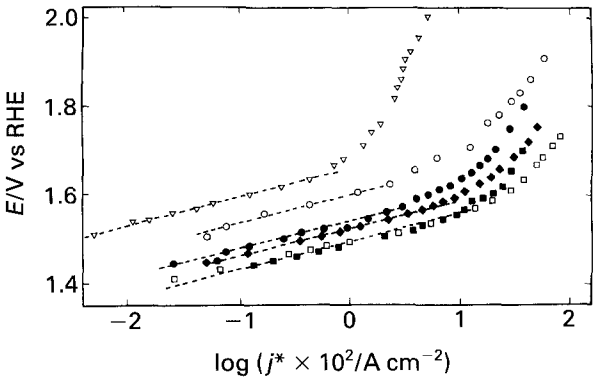

Fig. 3. Tafel plots derived from o.e.r. polarization curves at different NaOH concentrations and temperatures. Oxide coated G-16: 0.1 M, 30° C (▽); 1 M, 30° C (●); 4 M, 30° C (□); 1 M, 50° C (◆); 1 M, 80° C (■). Untreated G-16: 1 M, 30° C (○).

Table 1. Tafel slopes and apparent exchange current densities for the OER on oxide coated G-16 amorphous alloy at different NaOH concentrations and temperatures

c/M	T/K	b_T/V dec^{-1}	j_0^*/A cm^{-2}
0.1	303	0.06 ± 0.005	2.0×10^{-10}
1.0†	303	0.06 ± 0.005	7.5×10^{-10}
1.0	303	0.06 ± 0.005	4.4×10^{-9}
4.0	303	0.06 ± 0.005	1.3×10^{-8}
1.0	323	0.06 ± 0.005	4.7×10^{-9}
1.0	353	0.06 ± 0.005	6.9×10^{-9}

† Untreated G-16 amorphous alloy

different experimental conditions are assembled in Table 1. The values of j_0^* increase by two orders of magnitude as the NaOH concentration is increased from 0.1 to 4 M and about 55% as the temperature is raised from 30 to 80° C.

The potentials at different current densities in the low potential range were plotted as a function of the OH^- activity by using the activity data for aqueous NaOH [14, 15]. The plots give a slope of 0.12 V dec^{-1} (Fig. 4).

At constant potential in the Tafel region linear $\log j^*$ against log NaOH activity relationships were obtained (Fig. 5). From the slope of these plots $\delta \log j^*/\delta \log a_{NaOH} = 2.3 \pm 0.2$, it may be concluded that the rate of the o.e.r. at oxide coated G-16 in NaOH solution fits a second order reaction with respect to OH^- ions.

The apparent o.e.r. activation energy ΔH^* was calculated from Arrhenius plots obtained at a constant potential in the Tafel region, i.e. $E = 0.68$ V vs SHE. Taking into account the changes in activity of 1 M NaOH with temperature, $\Delta H^* = 40 \pm 5$ kJ mol^{-1}, a figure which agrees with data reported for other amorphous alloys [7] and Co–Ni spinels [16]. It should be noted that the calculation of the apparent energy of activation at the reversible potential from j^* values would be imprecise due to the long extrapolation involved.

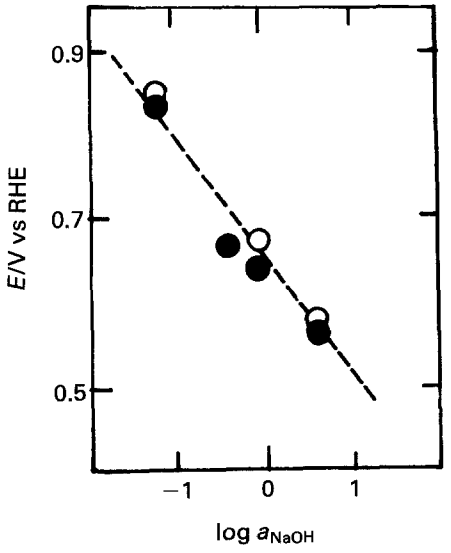

Fig. 4. Dependence of the potential on NaOH solution activity at $j^* = 1.0 \times 10^{-4}$ A cm^{-2} (●) and $j^* = 2.5 \times 10^{-4}$ A cm^{-2} (○); 30° C.

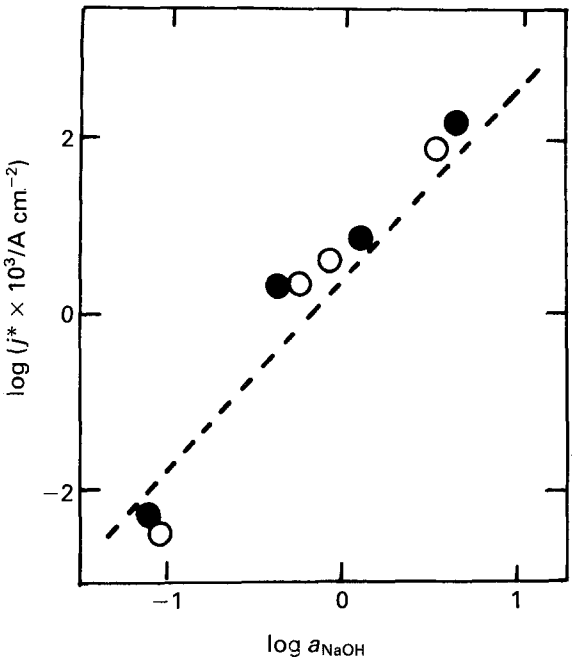

Fig. 5. Dependence of the current density on the activity of the OH^- ion at $E = 0.73$ V vs SHE (●), and $E = 0.75$ V vs SHE (○), 30° C.

3.2. *Departure from the Tafel behaviour*

The E against $\log j^*$ curves depart from the Tafel line at E_t, a threshold potential value which increases as both NaOH concentration and temperature are diminished. At potentials higher than E_t, gas bubbles are easily evolved from the electrode surface. Under these conditions linear E against j^* plots are obtained. The slopes of these lines are dependent on the NaOH concentration (Fig. 6). From the slope value an apparent ohmic resistance, R_a, can be evaluated. The R_a value decreases on increasing NaOH concentration (Fig. 7).

3.3. *SEM micrographs*

SEM micrographs of electrode surfaces before o.e.r. measurements in 1 M NaOH, 30° C, reveal a cracked

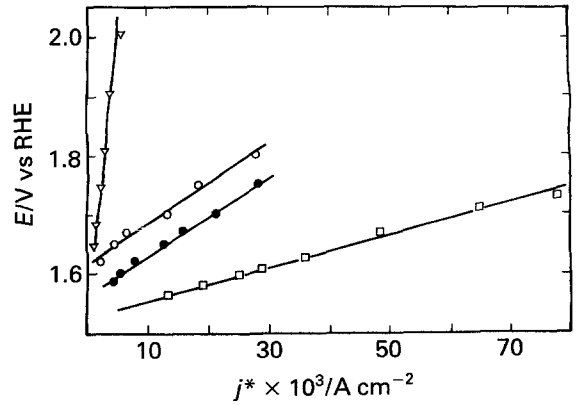

Fig. 6. O.e.r. polarization curves in the high overpotential region at different NaOH concentration; 30° C. Oxide coated G-16: 0.1 M (▽); 1 M (●); 4 M (□). Untreated G-16: 1 M (○).

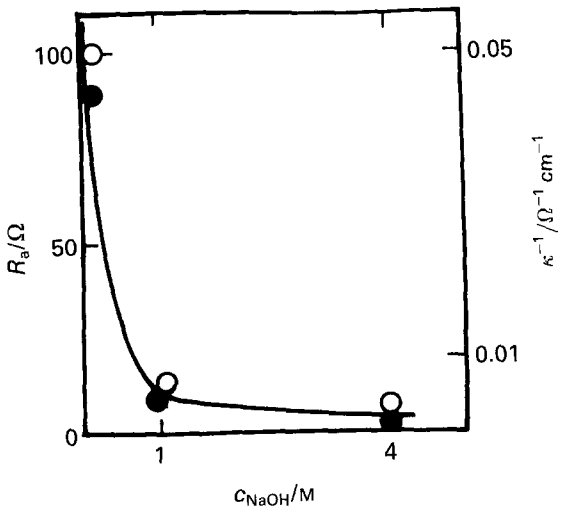

Fig. 7. Dependence of the apparent electrochemical resistance (R_a) (○), and the reciprocal of the specific conductance ($1/\kappa$) (●) on the NaOH concentration.

appearance, whereas after o.e.r. they show an irregular particle structure (Fig. 8).

6. Discussion

The kinetics of the oxygen evolution reaction in aqueous solutions at oxide film coated metal electrodes depends on the structure of the oxide film [17, 18], the oxidation state of the oxide film *at* or *near* the surface, the type of OH and O intermediates adsorbed at the oxide film surface [18] and the changes in the physicochemical properties of the metal oxide/solution interface caused by oxygen gas bubble formation [19]. The influence of each of these variables on the kinetics of the reaction depends on the applied potential.

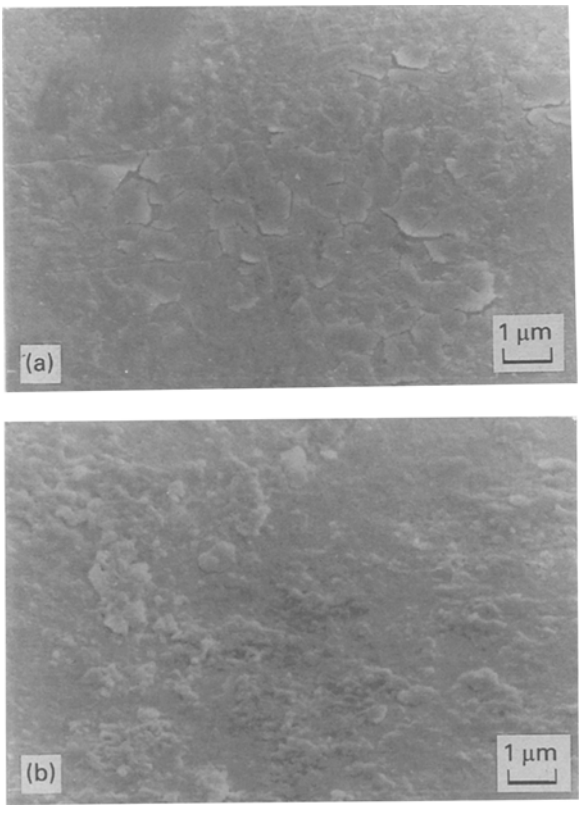

Fig. 8. Scanning electron micrographs of oxide coated G-16 before (a) and after (b) the o.e.r. measurements.

The application of a periodic perturbing potential routine of well defined conditions to either crystalline [20] or amorphous Co–Ni alloy [10] in NaOH solution promotes the growth of a hydrous oxide layer, which behaves as a precursor of a $NiCo_2O_4$ spinel, irrespective of nonmetallic components of the amorphous $Co_{50}Ni_{25}Si_{15}B_{10}$ alloy. Furthermore, present results show a better performance of oxide coated G-16 electrodes as compared to the G-16 itself for the o.e.r. in NaOH solutions. The high electrocatalytic activity of oxide coated G-16 may be assigned to the spinel-type structure of the electroformed metal oxide film. However, Burke and O'Sullivan have recently attributed the origin of the enhanced electrocatalytic activity of potential cycled metal electrodes towards the o.e.r. to the hydrous nature of the electroformed oxide film [21, 22]. Hydrous oxide layers formed on cobalt electrodes can be converted to spinel-type oxides by heating [23–25].

The mechanism of the o.e.r. on Ni, Co and their alloys has been thoroughly studied [5–9, 18, 19, 26–29]. For thermally prepared $NiCo_2O_4$, the o.e.r. polarization curves plotted as E against $\log j$, show two Tafel lines with slopes in the 0.04–0.06 V dec^{-1} range and in the 0.10–0.13 V dec^{-1} range, at low (l.c.d.) and high current density (h.c.d.), respectively [26–29]. Oxygen evolution takes place at potentials at which the electrode surface is already oxidized. Accordingly, the variation in Tafel slope has been explained considering a change in either the valence state of the metal oxide [27, 28], which implies a shift of active sites from di to trivalent sites [27], or coverage of the trivalent sites by reaction intermediates [29]. Likewise, the behaviour of the metal oxide coated electrodes produced by the application of periodic potential routines, varies with the base metal and the history of the metal oxide coating. Thus, the o.e.r. at aged oxide coated polycrystalline nickel electrodes has a single Tafel slope of about 0.05 V dec^{-1} [30], whereas oxide coated polycrystalline cobalt electrodes give two Tafel regions with slopes 0.03 and 0.12 V dec^{-1}, in the l.c.d. and h.c.d. ranges, respectively [25].

On the other hand, the polarization curves for the o.e.r. in alkaline solution on several amorphous alloys show two Tafel regions [7–9]. However, the o.e.r. at G-16 shows only the single Tafel slope, 0.06 V dec^{-1} [5, 6, 11]. In addition, electrochemical impedance spectroscopy of G-16 immersed in aqueous alkaline solutions shows two capacitive semicircles [11] in the impedance diagram in the o.e.r. potential range. The semicircle obtained at high frequency becomes almost potential-independent, and is associated with the electronic properties of the oxide layers, whereas the semicircle at low frequency becomes potential dependent, and is related to the response of O and OH adsorbed intermediates involved in the o.e.r.

Table 2. Theoretically predicted and experimentally obtained kinetic parameters for the OER on oxide coated G-16 samples in NaOH solution, 30° C

Kinetic parameter	*Theoretical*	*Experimental*
$(\partial E/\partial \log j^*)_{a_{OH^-}}$	2.3 (RT/F)	0.06 V dec^{-1}
$(\partial \log j^*/\partial \log a_{OH^-})_E$	2	2.3
$(\partial E/\partial \log a_{OH^-})_{j^*}$	2.3 $(-2RT/F)$	−0.12 V dec^{-1}

The kinetic parameters in Table 2 suggest that the o.e.r. at oxide coated G-16 in NaOH solutions in the Tafel region (low overpotential range) follows an extended and more complete version of the reaction pathway earlier proposed by Tamura *et al.* [31] for platinum in alkaline solution in l.c.d. conditions. The first step is OH^- ion discharge on an active site (S) yielding an absorbed (OH) species:

$$OH^- + S = S(OH) + e^- \quad (1)$$

followed by the formation of a surface oxide intermediate such as $S(O)^-$ [31] or $S(OH)_2^-$, according to

$$OH^- + S(OH) = S(O)^- + H_2O \quad (2a)$$

or

$$OH^- + S(OH) = S(OH)_2^- \quad (2b)$$

Step 2(b) explains the electrocatalytic efficiency of the hydrous metal oxide layers [21, 22]. Finally, the surface intermediate decomposition yields oxygen through reactions such as

$$S(O)^- + OH^- \Rightarrow O_2 + H^+ + S + 3e^- \quad (3a)$$

or

$$S(OH)_2^- \Rightarrow O_2 + 2H^+ + S + 3e^- \quad (3b)$$

Assuming that either Step 2(a) or (b) is rate-determining under Langmuir adsorption conditions, j, the o.e.r. current density can be written as

$$j = nF\left(\frac{k_1 k_2}{k_{-1}}\right) a_{OH^-}^2 \exp\left(\frac{FE}{RT}\right) \quad (4)$$

where k_1, k_{-1} and k_2 are the rate constants of Step 1 in the forward and backward direction, and Step 2 in the forward direction, respectively. At constant OH^- concentration, Equation 4 satisfies a Tafel relationship with slope $2.3(RT/F)$. Likewise, at constant potential, a second order reaction with respect to OH^-, and at constant current density, $(\partial E/\partial \log a_{OH^-}) = -2RT/F$, should be fulfilled. Experimental kinetic parameters are in close agreement with the predictions of this mechanism (Table 2).

For thermally prepared $NiCo_2O_4$ spinels with a random surface cation distribution, two surface cations are considered to be responsible for the o.e.r., being predominantly cobalt ions occupying tetrahedrical sites or two octahedrally located ions, which can be either cobalt or nickel ions [28]. This explanation probably applies to the Co–Ni spinel precursor layer built up on the G-16 surface. However, the o.e.r. kinetics at low overpotential may imply a synergetic effect due to simultaneous presence of cobalt and nickel ions at the oxide surface, and the hydrous characteristics of the oxide coating, which may assist the formation of $(OH)_2^-$-type intermediates.

The o.e.r. polarization curve at high overpotentials deviates from the $2.3(RT/F)$ slope. This departure occurs at a certain overpotential value which increases as the NaOH concentration decreases. At high overpotential linear E against j^* relationships are obtained; the slope of these lines increases as the resistivity of the solution increases.

Several authors have reported a departure from Tafel behaviour due to ohmic effects in the oxide films [30, 32], gas evolution [19] and/or diffusion control [33]. Nevertheless, when plotting E against j for that region, linear relationships are also observed [9, 19, 30, 33].

The influence of the ohmic resistivity of the oxide coating should be disregarded as results show that the slope of the linear E against j plot remains the same for both G-16 and oxide coated G-16. The interpretation based upon gas bubble formation appears to be most appropriate for the results of o.e.r. at G-16 and oxide coated G-16. Gas bubble formation reduces the available active surface area and an additional resistance arises which becomes rate controlling for the overall process at high overpotentials. This idea is supported by the following facts:

(i) The ohmic resistance evaluated from E against j^* curves at different NaOH concentrations follows the same dependence as the reciprocal of specific conductance with NaOH concentration (Fig. 7).

(ii) The o.e.r. Tafel behaviour departure occurs at an overpotential corresponding to the threshold potential for gas bubble evolution. This overpotential is mainly determined by the nature of the electrode/electrolyte solution interface.

Summarizing, the superior performance of metal oxide coated G-16 can be related to the catalytic influence of the hydrous metal oxide coating acting as a precursor of a Co–Ni spinel structure. For stabilized hydrous oxide films of thicknesses in the 30 to 50 nm range, their o.e.r. electrocatalytic activity in alkaline solutions becomes independent of the amount of hydrous oxide accumulated on the amorphous metal. Undoubtedly, the determining factors for the improved o.e.r. electrocatalytic activity are the surface composition and/or structure of the electrode material. Likewise, when the working area is restricted to the external surface, the roughness and/or porosity of the electrodes have little influence on their electrochemical performance [34, 35].

Acknowledgements

This project was financially supported by the Consejo Nacional de Investigaciones Científicas y Técnicas, Argentina. T. Kessler is a researcher of the Comisión de Investigaciones Científicas de la Provincia de Buenos Aires. The authors thank Professor G.

Kreysa, Dechema Institut, Frankfurt/M, Germany, for providing the amorphous metal specimens used in this work.

References

[1] M. D. Archer, C. C. Corke and B. H. Harji, *Electrochem. Acta* **32** (1987) 13.
[2] A. Baiker, *Faraday Discuss. Chem. Soc.* **87** (1989) 239.
[3] P. C. Searson, P. V. Nagarkar and R. M. Latanision, *in* 'Modern Aspects of Electrochemistry', Vol. 21 (edited by R. E. White, J. O'M. Bockris and B. E. Conway), Plenum Press, New York (1990) p. 121.
[4] G. A. Tsirlina, O. A. Petrii and N. S. Kopylova, *Elektrokhimiya* **26** (1990) 1059.
[5] G. Kreysa and B. Hakansson, *J. Electroanal. Chem.* **201** (1986) 61.
[6] H. Alemu and K. Jüttner, *Electrochim. Acta* **33** (1988) 1101.
[7] L. Vracar and B. E. Conway, *ibid.* **35** (1990) 1919.
[8] K. Lian, S. J. Thorpe and D. W. Kirk, *ibid.* **36** (1991) 537.
[9] *Idem*, *ibid.* **37** (1992) 2029.
[10] T. Kessler, W. E. Triaca and A. J. Arvia, *J. Appl. Electrochem.* **23** (1993) 655.
[11] T. Kessler, J. R. Vilche, M. Ebert, K. Juttner and W. J. Lorenz, *Chem. Eng. Technol.* **14** (1991) 263.
[12] R. S. Jev, J. Orehotsky, W. Visscher and S. Srinivasan, *J. Electrochem. Soc.* **128** (1981) 1900.
[13] M. Hamdani, J. F. Koenig and P. Chartier, *J. Appl. Electrochem.* **18** (1988) 561.
[14] H. S. Harned and J. C. Hecker, *J. Am. Chem. Soc.* **55** (1933) 4838.
[15] G. Akerlof and G. Kegeles, *ibid.* **62** (1940) 620.
[16] S. M. Jasem and A. C. C. Tseung, *J. Electrochem. Soc.* **126** (1979) 1353.
[17] S. Trasatti, *Electrochim. Acta* **29** (1984) 1503.
[18] T. C. Liu and B. E. Conway, Proceedings of the Second Symposium on Electrode Materials and Processes for Energy Conversion and Storage (1987), p. 307.
[19] R. N. Sing, M. Hamdeni, J. F. Koenig, G. Poillerat, J. L. Gauthier and P. Chartier, *J. Appl. Electrochem.* **20** (1990) 442.
[20] M. R. G. de Chialvo and A. C. Chialvo, *Electrochim. Acta* **36** (1991) 1963.
[21] L. D. Burke and E. J. M. O'Sullivan, *J. Electroanal. Chem.* **117** (1981) 155.
[22] L. D. Burke and M. E. G. Lyons, *in* 'Modern Aspects of Electrochemistry', Vol. 18 (edited by R. E. White, J. O'M. Bockris and B. E. Conway), Plenum Press, New York (1986) p. 169.
[23] T. Kessler, A. Visintin, M. R. de Chialvo, W. E. Triaca and A. J. Arvia, *J. Electroanal. Chem.* **261** (1989) 315.
[24] T. Kessler, A. Visintin, W. E. Triaca, A. J. Arvia and M. R. G. de Chialvo, *J. Appl. Electrochem.* **21** (1991) 516.
[25] M. R. G. de Chialvo and A. C. Chialvo, *Electrochim. Acta* **35** (1990) 437.
[26] C. R. Davidson, G. Kissel and S. Srinivasan, *J. Electroanal. Chem.* **132** (1982) 129.
[27] P. Rasiyah and A. C. C. Tseung, *J. Electrochem. Soc.* **130** (1983) 2384.
[28] D. B. Hibbert and C. R. Churchill, *J. Chem. Soc. Faraday Transac. 1* **80** (1984) 1965.
[29] J. Haenen, W. Vischer and E. Barendrecht, Extended Abstracts, 36th ISE Meeting, Salamanca, Spain (1985), Abstr. 02230.
[30] M. R. G. de Chialvo and A. C. Chialvo, *Electrochim. Acta* **33** (1988) 825.
[31] C. Iwakura, K. Fukuda and H. Tamura, *ibid.* **21** (1976) 501.
[32] C. D. Cahan and C. T. Chen, 'Extended Abstracts', Spring Meeting of The Electrochemical Society, Minneapolis, USA (1981) p. 1260.
[33] K. K. Lian and B. I. Birss, *J. Electrochem. Soc.* **138** (1991) 2885.
[34] H. Wendt and V. Plzak, *Electrochim. Acta* **28** (1983) 27.
[35] S. P. Jiang and A. C. C. Tseung, *J. Electrochem. Soc.* **138** (1991) 1216.